Journal of Molecular Structure 971 (2010) 39–46

Contents lists available at ScienceDirect

Journal of Molecular Structure

journal homepage: www.elsevier.com/locate/molstruc

Vibrational assignment and proton tunneling in pyridine–pyridinium complexes

Sayyed Faramarz Tayyari [a,*], Sayyed Jalil Mahdizadeh [a], Soheila Holakoei [a], Yan Alexander Wang [b,**]

[a] Department of Chemistry, Ferdowsi University of Mashhad, Mashhad 91775-1436, Iran
[b] Department of Chemistry, University of British Columbia, Vancouver, Canada BC V6T 1Z1

ARTICLE INFO

Article history:
Received 15 December 2009
Received in revised form 3 March 2010
Accepted 4 March 2010
Available online 10 March 2010

Keywords:
Pyridine–pyridinium complex
Proton tunneling
Hydrogen bonding
Vibrational spectra

ABSTRACT

The pyridine–pyridinium cationic complexes [$(Py_2H)^+$], with two different counterions (perchlorate and bromide), were prepared. The vibrational spectra of the complexes have been recorded. We then performed theoretical calculations to aid our understanding of the experimental data. To include the proton tunneling effect in our study, we adopted a simple one-dimensional potential energy surface (PES) for the motion of the hydrogen atom (at the center). This PES was derived from quantum mechanical calculations at the B3LYP/6-311++G** level of theory for a fixed skeleton geometry. Based on such a PES, we computed the vibrational energy levels, from which a tunneling splitting of 487 ± 2 and 242 ± 2 cm^{-1} was obtained in the gas and solution phases, respectively. The calculated barrier height was about 2.0–2.3 and 4.0–4.2 kcal/mol in the gas and solution phases, respectively. After all things considered, our calculations assign the bands at 138, 1255, and 1665 cm^{-1} to the N···N stretching, N–H out-of-plane bending, and N–H in-plane bending modes, respectively.

1. Introduction

Hydrogen bond is one of the most common binding mechanisms in nature. The strength of hydrogen bond has been estimated to be in the range of 4–160 kJ/mol [1]. Hydrogen-bonded systems have been studied by several spectroscopic techniques. Among them, vibrational spectroscopy plays an important role, the observed vibrational wavenumbers provide strong evidence for estimating the strength of hydrogen bond [2]. Theoretical calculations of hydrogen-bond strength, in conjunction with vibrational spectroscopy, often offer critical assistance in the interpretation of the existing experimental results and understanding the nature of hydrogen-bonded systems [3,4].

Pyridine (azabenzene) has attracted a lot of attention owing to its applications in many areas of chemistry. In particular, it has been used very frequently as a proton acceptor in studies involving hydrogen-bonded complexes [5–8]. Several substituted pyridine–pyridinium complexes have been studied both experimentally and theoretically [7,8]. In this study, pyridine–pyridinium complex, with a relatively simple intermolecular hydrogen bond, has been chosen as the model system, whose proton movement possesses either a symmetric double minimum or a symmetric single minimum hydrogen-bond potential.

The goals of the present work are reconsidering the vibrational assignment and studying the nature of the hydrogen-bonded system in the pyridine–pyridinium complex by means of density functional theory (DFT). For comparison, the harmonic and anharmonic vibrational frequencies of pyridine in the gas phase and in solution were also calculated. The resulting vibrational assignment will be compared with those reported in the literature [7,8].

2. Method of calculations

All calculations of geometry optimizations and vibrational frequencies in the present study were performed using Gaussian 03 package [9] in both gas and solution phases. Modern DFT method with the Becke three-parameter hybrid functional, B3LYP [10–12], was selected. Among various basis sets, B3LYP/6-311++G** was shown to be the superior choice for the estimation of the potential surface of hydrogen-bonded systems [3,4].

The solvent effect of pyridine–pyridinium cation complex was explored by adopting the Onsager reaction model in a self-consistent reaction field (SCRF) [13,14] (using the dielectric constant of pyridine, 12.5 [15]). The harmonic and anharmonic vibrational frequencies of pure pyridine in the gas phase were calculated at the B3LYP level, using 6-311++G** and 6-31G** basis sets, respectively.

Optimized geometries, vibrational frequencies, and the potential surfaces of the pyridine and pyridine–pyridinium complex were calculated at the B3LYP/6-311++G** level. The assignment of the calculated frequencies was aided by the animation option of GaussView 3.0 graphical interface [16] for the Gaussian programs [9], which gives a visual presentation of the vibrational modes.

* Corresponding author. Tel.: +98 511 8780216; fax: +98 511 8438032.
** Corresponding author.
E-mail addresses: tayyari@ferdowsi.um.ac.ir (S.F. Tayyari), yawang@chem.ubc.ca (Y.A. Wang).

0022-2860/$ - see front matter © 2010 Elsevier B.V. All rights reserved.
doi:10.1016/j.molstruc.2010.03.014

To explore the proton tunneling, we have varied the N–H distance from 0.9 Å to the midpoint between the two nitrogen atoms in both gas phase and solution and calculated the energies by B3LYP/6-311++G** while fixing all other structural parameters at their optimized equilibrium values. The potential energy surfaces obtained at these levels were fitted to the following anharmonic one-dimensional potential function:

$$2V = K_2X^2 + K_4X^4, \quad (1)$$

using Genplot package [17], where K_2 and K_4 represent the quadratic and quartic force constants in the N–H stretching mode, respectively.

The above symmetric double-minimum potential function is introduced into the Hamiltonian for a linear triatomic system [3,4,18,19],

$$\hat{H} = 1/2[K_2\mu Q^2 + K_4\mu^2 Q^4 + P^2], \quad (2)$$

where Q is the mass weighted coordinate in the stretching direction, μ is the reduced mass of the system, and P is the corresponding momentum. Despite that this simple Hamiltonian does not takes into account of possible interaction with the N···N stretching and N–H bending, our theoretical results indeed produce a good agreement with experimental data (as clearly shown in Section 4 below).

Then, the wave function could be expressed in terms of the orthonormal harmonic oscillator wave functions:

$$\Psi_r = \sum_i a_i^r \Phi_i(Q), \quad (3)$$

where $\{a_i^r\}$ are the wave function expansion coefficients. Substitution of Ψ_r into the Schrödinger equation, $\hat{H}\Psi_r = E\Psi_r$, multiplying both sides by $\Phi_k^*(Q)$, and integrating over Q, we arrive at

$$\sum_i a_i^r H_{k,i} = E_r a_k^r, \quad (4)$$

where

$$H_{k,i} = \int_{-\infty}^{\infty}\int_{-\infty}^{\infty} \Phi_k^*(Q)\hat{H}\Phi_i(Q)dQ = \langle k|\hat{H}|i\rangle.$$

Rearrangement of Eq. (4) gives

$$\sum_i a_i^r(H_{k,i} - E_r\delta_{k,i}) = 0, \quad (5)$$

where $i, k = 0, 1, 2, \ldots, N$.

The non-trivial solutions of Eq. (5) are obtained from setting the determinant of the coefficient of a_i^r to zero [3]. The matrix elements $H_{k,i}$ are simple algebraic expressions involving indexes i,k and available tabulated potential parameters [20]. The resultant matrix of the order of 30×30 can then be readily diagonalized utilizing Microsoft FORTRAN power station V.1.

3. Experimental details

Pure pyridine was obtained from Aldrich. Perchlorate, sulfuric acids, sodium bromide, ethanol, methanol, and acetone were obtained from Merk. Pyridine was dried over barium oxide and redistilled. All salts and deuterated products were dried under vacuum in the presence of P_2O_5.

In order to prepare the pyridine–pyridinium complex with perchlorate counterion, perchloric acid (90%) was first added slowly to liquid pyridine to obtain pyridinium perchlorate salt ($PyHClO_4$) as a white precipitate, which was recrystallized from 90% ethanol [21]. This salt was dried under vacuum and then dissolved in pure pyridine to give a 2 M solution.

In order to prepare the pyridine–pyridinium complex with bromide counterion, an ether solution of pyridine was treated with anhydrous HBr to give pyridinium bromide salt (PyHBr) as a white solid, which was recrystallized from a methanol–acetone mixture [21]. This salt was dried under vacuum and then it was dissolved in pure pyridine to give a 2 M solution. Anhydrous HBr was produced by adding sulfuric acid (>99%) to sodium bromide.

Deuterated salt was prepared by twice exchanging with D_2O, and the excess was pumped off by vacuum and dried under vacuum condition. Then, it was dissolved in pure pyridine to obtain 2 M deuterated pyridine–pyridinium complex [$(Py_2D)^+$] solution [7].

The mid-IR spectra of [$(Py_2H)^+$] and [$(Py_2D)^+$] solutions were recorded on a Bomem MB-154 Fourier transform spectrophotometer in the region 4000–500 cm^{-1} by averaging 20 scans with a resolution of 20 cm^{-1}. The Far-IR spectra in the region 600–100 cm^{-1} were obtained using a Thermo Nicolet NEXUS 870 FT-IR spectrometer equipped with DTGS/polyethylene detector and a solid substrate beam splitter. The spectrum was collected with a resolution of 2 cm^{-1} by averaging the results of 64 scans.

The Raman spectra were recorded employing a 180° back-scattering geometry and a Bomem MB-154 Fourier transform Raman spectrometer. It was equipped with a ZnSe beam splitter and a TE cooled InGaAs detector. Rayleigh filtration was afforded by two sets of two holographic technology filters. The spectra were collected with a resolution of 2 cm^{-1} by coadding the results of 220 scans. The laser power at the sample was 400 MW.

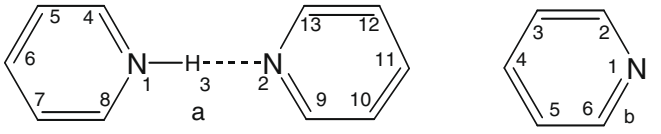

Fig. 1. Numbering system and geometry of pyridine–pyridinium complex (a) and pyridine (b).

Table 1
The geometrical parameters of $(Py_2H)^+$ and pyridine.

	$(Py_2H)^+$		Pyridine		
	Gas[a]	Solution[a]	Calc.[a]	Calc.[b]	Expt.[b]
Bond lengths (Å)					
N1···N2	2.687	2.763			
N1–H3	1.107	1.076			
H3···N2	1.580	1.687			
N1–C4/N1–C8	1.345	1.346	1.337	1.329	1.338
C4–C5/C7–C8	1.384	1.383	1.394	1.382	1.394
C5–C6/C6–C7	1.395	1.396	1.392	1.383	1.392
N2–C9/N2–C13	1.343	1.342			
C9–C10/C12–C13	1.389	1.390			
C10–C11/C11–C12	1.393	1.392			
Bond angles (°)					
N–H3–N2	180.0	180.0			
H3–N1–C4/H3–N1–C8	119.1	119.0			
C4–N1–C8	121.8	122.0	117.3	119	116.9
N2–C4–C5/N2–C8–C7	120.4	120.2	123.6	122.4	123.8
C4–C5–C6/C6–C7–C8	118.8	118.9	118.5	118.6	118.5
C5–C6–C7	119.7	119.8	118.5	119	118.4
H3–N2–C9/H3–N2–C13	120.7	120.7			
C9–N2–C13	118.6	118.3			
N2–C9–C10/N2–C13–C12	122.6	122.8			
C9–C10–C11/C11–C12–C13	118.6	118.6			
C10–C11–C12	119.0	118.9			
Φ[c]	90.0	90.0			

[a] Calculated at the B3LYP/6-311++G**.
[b] Data from Ref. [10].
[c] Φ, the dihedral angle between the pyridine and pyridinium rings.

4. Results and discussion

4.1. Geometrical structures and frequencies

The geometrical parameters of pyridine–pyridinium complex (Fig. 1a) and pyridine calculated at the B3LYP/6-311++G** level in both gas and solution phases are listed in Table 1.

As it is shown in Table 1, the N···N distance of pyridine–pyridinium (Fig. 1a) in solution is considerably longer than that in the gas phase (0.076 Å) and the N–H bond length in the gas phase is considerably longer than that in solution (0.031 Å). These results indicate that the hydrogen-bond strength in solution is significantly weaker than that in the gas phase. Such a conclusion agrees with the report by Fritsch and Zundel [8] whose experiment showed that the strength of hydrogen bond of this system is very sensitive to the media. The N···N, N–H and N···H calculated distances are in agreement with those reported by Shenderovich [24] and Guzei et al. [25]. Furthermore, as indicated in Table 1, our calculated structural parameters for pure pyridine are more accurate than those reported by Wiberg et al. [22].

The hydrogen bond energies, E_{HB}, were calculated according to the following equation:

$$E_{HB} = E_{PyHPy} - (E_{PyH} + E_{Py}). \quad (6)$$

The calculated E_{HB} was 104.2 and 80.7 kJ/mol in the gas and solution phases, respectively, which is in agreement with the value (98.2 kJ/mol) reported by Shenderovich [24].

The calculated and observed vibrational frequencies and their assignments for pyridine, $[(Py_2H)^+]$, and $[(Py_2D)^+]$ are shown in Tables 2–4, respectively, which are compared with previous results and assignments reported by Clements and Wood [7] and by Urena et al. [23].

Table 2
The assignments of the vibrational frequencies (in cm^{-1}) of pyridine.[a]

Sym.	Theoretical				Experimental					Assignments		
	F_{an}	F	I_{IR}	I_R	IR	Raman	IR [7]	IR [21]	R [21]	T.W.	Ref. [7]	Ref. [2]
A1	3066	3194	7	286					3090 *w*	2		
B2	3083	3186	25	36	3033 *sh*			3033 *m*	3037 *sh*	20b		20b
A1	3052	3170	5	101	3053 *w*			3052 *m*	3057 *s*	7a		20a
A1	3014	3150	4	83	3076 *m*			3078 *m*	3072 *sh*	13		13
B2	3029	3147	28	100	3025 *m*			3025 *m*	3025 *sh*	7b		7b
A1	1600	1623	24	14	1581 *s*	1581 *m*	1583	1581 *vs*	1582 *w*	8a		8a
B2	1593	1617	10	9	1574 *sh*	1573 *m*	1572	1574 *s*	1574 *w*	8b		8b
A1	1493	1510	2	2	1482 *s*	1483 *w*	1482	1482 *s*	1483 *w*	19a	19a	19a
B2	1453	1470	27	0	1438 *vs*		1439	1437 *vs*		19b	19b	19b
B2	1360	1384	0	0						3		
B2	1257	1284	0	2						14		
A1	1229	1241	5	8	1217 *m*	1217 *w*	1218	1216 *m*	1218 *w*	9a		9a
B2	1163	1170	2	2	1148 *m*	1146 *vw*	1148	1146 *m*	1147 *vw*	15	15	15
A1	1078	1093	5	1	1068 *m*	1066 *vw*	1068	1068 *m*	1069 *vw*	18a	18a	18b
B2	1059	1076	0	0			1085			18b	18b	
A1	1034	1047	6	35	1030 *s*	1030 *vs*	1030	1030 *s*	1031 *s*	12	12	12
B1	993	1010	5	30	991 *s*	992 *vs*	993	991 *s*	991 *vs*	1	1	1
A1	996	1006	0	0						5		
A2	978	996	0	0						17a		
B1	939	954	1	0	941 *w*			942 w		10b		10b
A2	882	892	1	0	887 *w*			884 w	881 *vw*	10a		10a
B1	752	758	12	0	748 *s*		749	748 s	750 *vw*	4	10b	4
B1	708	715	67	0	705 *vs*		703	701 vs		11	11	11
B2	663	669	0	5		653 *w*	652	653 vw	654 *w*	6b	6b	6b
A1	606	616	4	4	603 *s*	603 *w*	605	603 s	604 *w*	6a	6a	6a
B1	413	417	4	0		408 *vw*		406 s	407 *vw*	16b		16b
A2	377	381	0	0						16a		

[a] F_{an} and F stand for anharmonic and harmonic vibrational frequencies, calculated at the B3LYP using 6-31G** and 6-311++G** basis sets, respectively; I_{IR} and I_R stand for relative IR and Raman intensities, respectively; the roman characters after wavenumbers describe the features of the observed peaks; *v*, very; *w*, weak; *m*, medium; *s*, strong; *sh*, shoulder; vibrational assignments for the pyridine ring are given in the Wilson notation; T.W. this work.

Table 3
The assignments of the vibrational frequencies (in cm^{-1}) of $(Py_2H)^+$.

No.	Theoretical[a]			Experimental[b]				Assignments[c]		
	v	I_{IR}	I_R	IR	Raman	IR [7]	Raman [7]	Gas	Solution	Ref. [7]
1	3223/3224	0/1	312/81	3078*w*	3087*vw*			2(1)	2(1)	
2	3220/3222	3/8	15/54	3078*w*	3087*vw*			20b(1)	20b(1)	
3	3212/3213	0/8	279/174	3053*w*	3058*vs*			2(2)	20a(1)	
4	3210/3211	3/0	9/1	3053*w*	3058*vs*			20a(1)	7b(1)	
5	3208/3208	0/1	78/43	3031*w*	3037 *sh*			7b(1)	2(2)	
6	3207/3103	1/5	53/80	3031*w*	3037*sh*			20b(2)	20b(2)	
7	3197/3198	0/0	73/3	3025*w*	3027*sh*			13(1)	13(1)	
8	3191/3186	1/4	76/107	3025*w*	3027 *sh*			7a(2)	7a(2)	
9	3172/3171	2/2	62/169	3000*w*				13(2)	13(2)	
10	3170/3169	7/91	54/15	3000*w*				7b(2)	7b(2)	
11	2049/2475	5404/6864	380/1635	2080–2540		2080–2530		ν_{NH}	ν_{NH}	ν_{NH}
12	1713/1705	27/36	3/27	1665 *m*				$\delta_{NH} + \nu_{as(C=C)}$	δ_{NH}	
13	1659/1661	4/12	23/54	1635*w*	1635*w*	1639 *m*	1635	8a(1)	8a(1)	8a

(*continued on next page*)

Table 3 (*continued*)

No.	Theoretical[a]			Experimental[b]				Assignments[c]		
	v	I_{IR}	I_R	IR	Raman	IR [7]	Raman [7]	Gas	Solution	Ref. [7]
14	1643/1640	109/110	20/143	1598 m	1598 *m*	1603 *m*		8a(2)	8a(2)	8b
15	1618/1617	4/6	11/42	1574 *sh*	1572 *m*			8b(2)	8b(2)	
16	1597/1583	5/10	6/83	1537 *m*		1549 *m*		8b(1)	8b(1) + δ_{NH}	19b
17	1520/1519	42/0	0/39					19a(1)	19a(2)	
18	1517/1518	42/77	1/55	1489 *s*		1493 *s*		19a(2)	19a(1)	19a
19	1487/1478	47/55	0/52	1483 *sh*	1483 *w*			19b(2)	19b(2)	
20	1449/1444	21/25	1/0	1439 *vs*				19b(1)	19b(1) + δ_{NH}	
21	1391/1390	3/2	0/1					3(2)	3(2)	
22	1373/1371	7/10	0/0					3(1)	3(1)	
23	1362/1261	2/15	0/68	1255 *w*		1255 *m*	1260	γ_{NH}	γ_{NH}	δ_{NH}
24	1309/1309	3/3	1/3					14(1)	14(1)	
25	1290/1301	3/1	1/27					14(2)	14(2)	
26	1239/1241	14/22	7/3	1217 *m*	1218 *w*			9a(2)	9a(2)	
27	1225/1223	20/26	8/8	1203 *sh*		1205 *s*	1200 *sh*	9a(1)	9a(1)	9a
28	1192/1194	3/5	1/1	1155 *sh*				15(1)	15(1)	
29	1184/1180	3/4	2/4	1148 *m*	1149 *vw*	1167 *m*		15(2)	15(2)	15
30	1092/1090	42/40	4/50	1082 *s*		1087 *w*		18a(2)	18a(2)	18b
31	1091/1089	3/4	1/1					18b(1)	18b(1)	
32	1089/1086	1/1	0/4					18b(2)	18b(2)	
33	1085/1083	4/8	1/13	1061 *s*	1066 *vw*			18a(1)	18a(1)	
34	1060/1055	45/40	3/52	1038 *sh*	1033 *sh*	1040 *s*		12(2)	12(2)	18a
35	1040/1011	1/15	73/44	1032 *m*	1031 *vs*			1(1)	1(1)	
36	1039/1043	0/0	0/51	1032	1031 *vs*			5(1)	5(1)	
37	996/1041	122/7	48/33		1021 *s*		1024	12(1)	12(1)	12
38	1032/1023	0/3	0/68	991 *m*	991 *vs*			5(2)	5(2)	
39	1028/1027	85/98	49/40	1005 *m*	1005 *s*	1007 *s*	1010		1(2)	1
40	1007/1006	0/0	0/0					17a(1)	17a(1)	
41	1002/1002	0 /0	0/1					17a(2)	17a(2)	
42	968/965	1/1	0/1	931 *vw*		942 *m*	952	10b(1)	10b(1)	γ_{NH}
43	964/963	0/0	0/6	931				10b(2)	10b(2)	
44	899/898	0/0	0/8					10a(2)	10a(2)	
45	893/890	0/0	0/3	885 *vw*				10a(1)	10a(1)	
46	771/770	53/76	0/58	752 *s*		762*sh*	751	4(1)	4(1)	10b
47	767/764	28/30	0/257	752		762	751	4(2)	4(2)	
48	715/713	51/74	0/374	706 *s*				11(2)	11(2)	
49	696/691	39/53	0/416	685 *s*		684 *s*		11(1)	11(1)	11
50	664/665	0/0	5/89		653 *w*			6b(2)	6b(2)	
51	656/654	0/1	6/51		642 *sh*		650	6b(1)	6b(1)	6b
52	651/643	74/75	5/76		642			6a(2)	6a(2)	
53	603/611	71/33	8/26	603 *m*	603 *w*	628 *s*	630	6a(1)	6a(1)	6a
54	423/422	3/4	0/120		408 *w*			16b(2)	16b(2)	
55	417/412	1/1	0/72					16b(1)	16b(1)	
56	401/402	0/0	0/12					16a(1)	16a(1)	
57	392/391	0/0	0/18					16a(2)	16a(2)	
58	137/118	69/74	0/3			138		νN···H–N	νN···H–N	νN···H–N
59	134/130	0/0	2/2					δN···H	δN···H	
60	116/107	3/5	1/8					γN···H	γN···H	
61	44/38	0/1	2/11					δ_{rings}	δ_{rings}	
62	43/36	0/0	3/11					δ_{rings}	δ_{rings}	
63	34/23	0/0	12/3					Rings torsion	Rings torsion	

[a] I_{IR} and I_R stand for relative IR and Raman intensities, respectively. The first and second numbers in each column are for gas and solution phases, respectively; *v*, δ, and γ stand for stretching, in-plane, and out-of-plane bending, respectively.

[b] The roman characters after wavenumbers describe the features of the observed peaks: *v* for very, *s* for strong, *m* for medium, *w* for weak, and *sh* for shoulder.

[c] Vibrational assignments for the pyridine ring are given in the Wilson notation. "(1)" and "(2)" refer to the pyridine ring closer to and far away from the central proton of the hydrogen bond, respectively.

Table 4
The assignments of the vibrational frequencies (in cm^{-1}) of $(Py_2D)^+$.[a]

	Theoretical			Experimental			Assignments		
	F	I_{IR}	I_R	IR [7]	IR [7]	Raman [7]	Gas	Solution	Ref. [7]
1	3223/3225	0/0	314/84	3078 *w*			2(1)	2(1)	
2	3220/3222	3/8	15/54	3078 *w*			20b(1)	20b(1)	
3	3212/3208	0/2	276/46	3052 *w*			2(2)	2(2)	
4	3210/3213	4/11	9/181	3052 *w*			20a(1)	20a(1)	
5	3208/3211	0/0	78/1	3030 *w*			7b(1)	7b(1)	
6	3207/3203	1/5	53/80	3030 *w*			20b(2)	20b(2)	
7	3197/3198	0/0	73/3	3026 *w*			13(1)	13(1)	
8	3191/3186	0/3	77/104	3026 *w*			7a(2)	7a(2)	
9	3172/3171	0/0	61/158	3000 *w*			13(2)	13(2)	
10	3170/3169	7/9	53/15	3000 *w*			7b(2)	7b(2)	
11	1575/1875	889/3204	104/643	1995 *m*	1920 *m*		ν_{ND} + $\nu_{C=C}$	ν_{ND}	
12	1695/1649	768/8	34/66	1589 *sh*	1637 *m*	1626	8a(1)	8a(1)	8a

Table 4 (*continued*)

	Theoretical			Experimental			Assignments		
	F	I_{IR}	I_R	IR [7]	IR [7]	Raman [7]	Gas	Solution	Ref. [7]
13	1644/1639	40/163	11/194	1581 *s*	1600 *m*		8a(2)	8a(2)	8b
14	1624/1622	3/3	9/18	1578 *sh*			8b(1)	8b(1)	
15	1616/1616	2/5	11/46	1572 *sh*			8b(2)	8b(2)	
16	1519/1519	3/1	0/36	1489 *sh*			19a(2)	19a(2)	
17	1515/1517	43/59	0/51	1483 *m*	1540 *m*		19b(1)	19b(1)	19b
18	1487/1510	891/181	42/100	1439 *vs*			19a(1) + ν_{ND}	19a(1)	
19	1480/1446	38/49	0/39	1439			19b(2)	19b(2)	
20	1389/1389	1/1	0/0				3(2)	3(2)	
21	1387/1387	0/1	0/2				3(1)	3(1)	
22	1337/1341	9/12	1/0			1304	14(1)	14(1)	3
23	1299/1292	0/1	0/2				14(2)	14(2)	
24	1239/1241	16/23	7/4	1217 *m*			9a(2)	9a(2)	
25	1225/1223	321/27	8/8	1205 *sh*	1206 *s*		9a(1)	9a(1)	9a
26	1192/1195	3/5	1/2				15(1)	15(1)	
27	1184/1180	3/4	2/4	1148 *s*	1170 *m*		15(2)	15(2)	15
28	1170/1166	0/0	0/13				δ_{ND} + 18b(1)	δ_{ND} + 18b(1)	
29	1101/1094	0/0	1/13				18b(2) + γ_{ND}	18b(2) + γ_{ND}	
30	1091/1090	43/41	3/47	1068 *s*	1079 *w*		18a(2)	18a(2)	18b
31	1084/1082	2/7	1/16	1039 *sh*			18a(1)	18a(1)	
32	1059/1055	39/35	4/52	1032 *s*	1037 *s*		12(2)	12(2)	18a
33	1045/1044	3/0	0/53				18b(1)	5(1)	
34	1040/1040	0/3	81/36				1(1)	1(1)	
35	1039/1034	0/4	0/13				5(1)	18b(1) + δ_{ND}	
36	1032/1023	0/7	0/67			1025	5(2)	5(2)	12
37	1028/1025	72/84	38/38	1005 *w*	1005 *s*	1007	1(1) + 12(2)	1(1) + 12(2)	1
38	1011/991	1/0	0/26				γ_{ND} + 10b(1)	γ_{ND} + 10b(1)	
39	1007/1006	0/0	0/0				17a(1)	17a(1)	
40	1002/1002	0/0	0/1				17a(2)	17a(2)	
41	964/963	0/0	0/5				10b(2)	10b(2)	
42	954/984	257/87	62/56	989 *s*			12(1)	12(1)	
43	941/905	1/1	0/35				10b(1)	10b(1) + γ_{ND}	
44	899/898	0/0	0/8	883 *vw*			10a(2)	10a(2)	
45	893/890	0/0	0/3	883			10a(1)	10a(1)	
46	767/764	28/30	0/251	762 *m*	762*sh*		4(2)	4(2)	10b
47	763/757	57/83	0/42	750 *vs*			4(1)	4(1)	
48	715/713	51/74	0/374	704 *vs*			11(2)	11(2)	
49	696/691	38/52	0/416	687 *m*	684 *s*		11(1)	11(1)	11
50	664/665	0/0	5/90			643	6b(2)	6b(2)	6b
51	656/653	0/1	5/51			643	6b(1)	6b(1)	6b
52	649/641	69/70	4/72	603 *m*	625 *s*	626	6a(2)	6a(2)	6a
53	588/601	111/54	11/36	603	585 br	590	6a(1)	6a(1)	Proton mode
54	422/422	3/4	0/120				16b(2)	16b(2)	
55	413/408	1/1	0/70				16b(1)	16b(1)	
56	401/402	0/0	0/12				16a(1)	16a(1)	
57	392/391	0/0	0/18				16a(2)	16a(2)	
58	136/117	68/73	0/3		136		νN···D–N	νN···D–N	νN···D–N
59	134/130	0/0	1/2				δN···D	δN···D	
60	116/106	3/5	1/8				γN···D	γN···D	
61	43/37	0/1	2/11				δ_{rings}	δ_{rings}	
62	42/36	0/0	3/11				δ_{rings}	δ_{rings}	
63	34/23	0/0	12/3				Rings torsion	Rings torsion	

[a] See footnotes of Table 3; br, broad.

The regions of the N–H and N–D stretching frequencies are shown in Figs. 2 and 3, respectively. The N–H stretching band is a strong, broad doublet with two maxima at 2080 and 2540 cm^{-1}. It has been shown that these features are independent of solvent or counterion [7]. Replacement of the hydrogen atom by deuterium completely changes the appearance of the infrared spectrum in this region. Deconvolution of the 1700–2300 cm^{-1} region suggests that it is combined from three sharp bands of pyridine itself and a broad and strong band at about 1995 cm^{-1} (assigned to the N–D stretching mode).

Deconvolution of the IR spectra of pyridine complexes at the 1800–1600 cm^{-1} region (Fig. 4) reveals the presence of four weak bands in this region. The weak band around 1665 cm^{-1}, which is absent in the deuterated analogous and pure pyridine IR spectra, is attributed to the N–H in-plane bending mode according to our calculations. A medium band near 1633 cm^{-1} (weak in pure pyridine) was attributed to a combination band $\nu_{12} + \nu_{6a}$ [23]. Clements

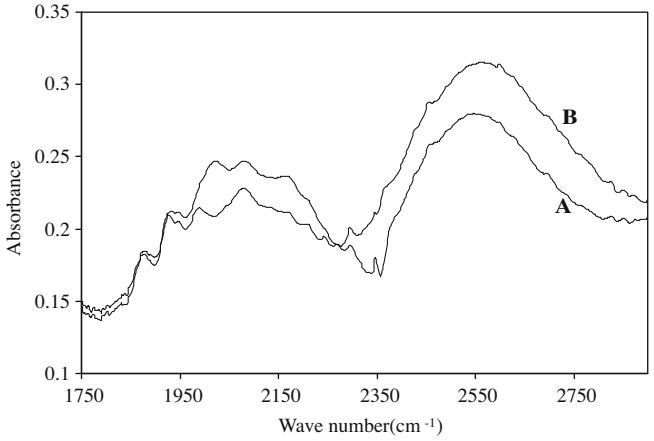

Fig. 2. NH stretching bands of $(Py_2H)^+Br^-$ (A) and $(Py_2H)^+ClO_4^-$ (B) in pyridine.

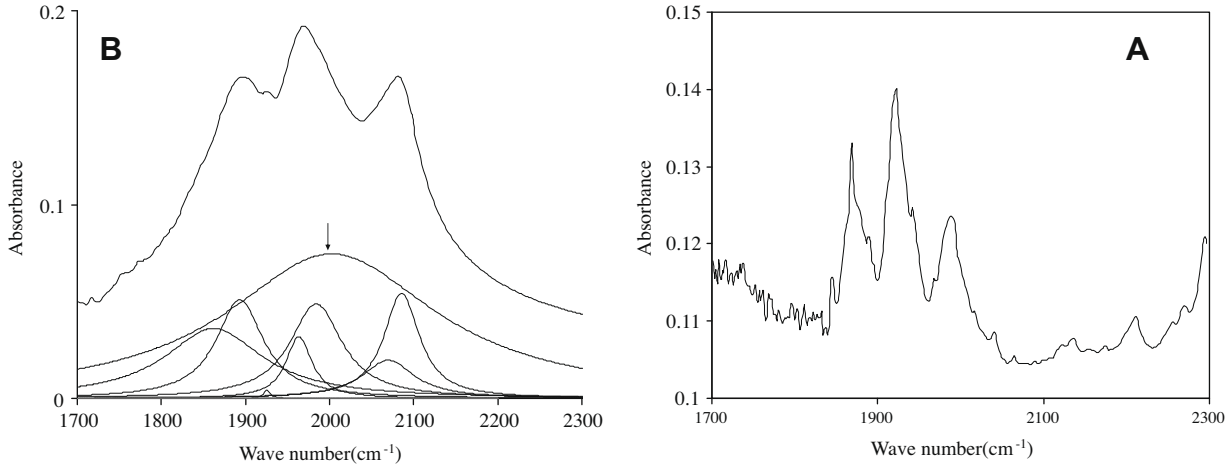

Fig. 3. Three sharp combination bands in pure pyridine (A) and the N–D stretching band in deconvoluted spectrum of $(Py_2D)^+ClO_4^-$ in pyridine (B).

and Wood [7] assigned the band at 1255 cm^{-1} to this vibrational mode. However, in our study, the 1255 cm^{-1} band, which disappears upon deuteration (Fig. 5), is assigned to the out-of-plane bending mode instead.

The two strong bands at 1099 and 625 cm^{-1} in the IR spectra of $(Py_2H)ClO_4$ (Fig. 6) are assigned to the asymmetric stretching and bending modes of ClO_4^{-1} ion, respectively.

Three important normal modes existing in the far infrared region are related to the intermolecular H···N vibrations. These normal modes are in-plane and out-of-plane N···H bending modes ($\delta_{N\cdots H}$ and $\gamma_{N\cdots H}$ in Tables 3 and 4) and N–H···N stretching mode ($\nu_{N-H\cdots N}$). The first two bands have not been observed but the third mode has been reported to occur at 138 and 136 cm^{-1} for the light and deuterated systems, respectively [7]. These results are in excellent agreement with our calculated results.

Unfortunately, the tunneling frequency has not been detected experimentally to be compared with our calculated results.

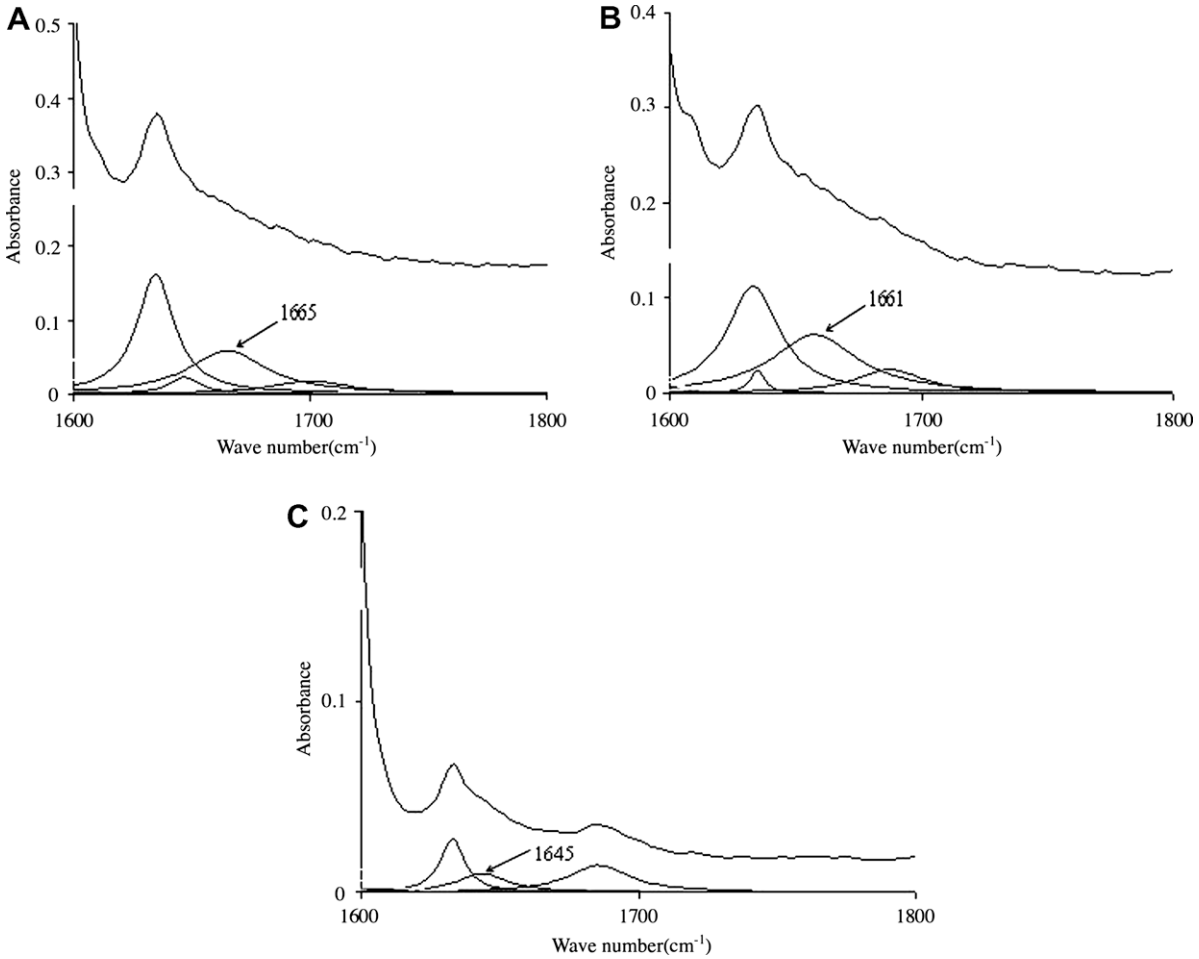

Fig. 4. In-plane NH bending of $(Py2H)^+Br^-$ (A) and $(Py_2H)^+ClO_4^-$ (B) in pyridine with the spectrum of $(Py_2D)^+ClO_4^-$ in pyridine (C) for comparison.

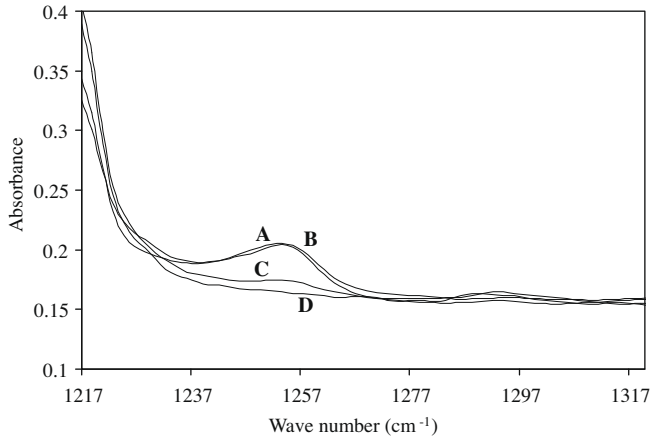

Fig. 5. Out-of-plane NH bending of $(Py_2H)^+ClO_4^-$ (A) and $(Py2H)^+Br^-$ (B) in pyridine with the spectra of $(Py_2D)^+ClO_4^-$ in pyridine (C) and pure pyridine (D).

4.2. Potential surfaces of pyridine–pyridinium cation complex

Tables 5 and 6 summarize the $|0\rangle_{\pm} \rightarrow |n\rangle_{\pm}$ transition frequencies for various cutoffs (restriction) imposed on the amplitude of hydrogen motion in the gas and solution phases for both hydrogen and deuterium systems, respectively. In these tables, "*n*" indicates the number of nodal lines of the wave function along the stretching direction. If the potential energies up to 1000 and 1500 cm^{-1} for the gas and solution phases, respectively, are included in the fit for calculating the potential parameters of Eq. (1), then a tunneling splitting of 485 and 241 cm^{-1} for the hydrogen system at the gas and solution phases, respectively, is obtained. As it is shown in Tables 5 and 6, various selections of the potential cutoff do not affect the results much.

Table 7 summarizes the calculated barrier height for pyridine–pyridinium complex in the gas and solution phases with different energy cutoffs. We found that the barrier height is also quite insensitive to the selected potential energy cutoff. The barrier height of the proton transfer in the gas phase (*ca.* 770 cm^{-1}) [24,26] is about half of that in solution (*ca.* 1400 cm^{-1}), which is caused by the much stronger hydrogen bond in the gas phase than in solution.

Table 5
Transition frequencies (in cm^{-1}) in the gas phase calculated at the B3lYP/6-311++G** level for different energy cutoffs (in cm^{-1}). The first and second numbers in each column of transition frequency are for the normal and deuterated systems, respectively.

Cutoff	$\|0\rangle_+ \rightarrow \|0\rangle_-$	$\|0\rangle_+ \rightarrow \|1\rangle_-$	$\|0\rangle_- \rightarrow \|1\rangle_+$
600	488/221	3143/2399	1259/1001
800	487/219	3150/2402	1264/1000
1000	485/217	3153/2404	1268/997
1200	483/215	3158/2405	1271/994
1400	480/211	3159/2407	1274/991
Expt.		2540/1955	

Table 6
Transition frequencies (in cm^{-1}) in solution calculated at the B3lYP/6-311++G** level for different energy cutoffs (in cm^{-1}). The first and second numbers in each column of transition frequency are for the normal and deuterated systems, respectively.

Cutoff	$\|0\rangle_+ \rightarrow \|0\rangle_-$	$\|0\rangle_+ \rightarrow \|1\rangle_-$	$\|0\rangle_- \rightarrow \|1\rangle_+$
1000	165/37	2600/2019	1370/1110
1200	133/36	2603/2022	1372/1113
1400	161/35	2601/2026	1376/1115
1600	161/35	2605/2033	1377/1108
1800	154/33	2621/2048	1405/1111
Expt.		2540/1955	

Table 7
Barrier heights (in cm^{-1}) in the gas phase and solution calculated at the B3lYP/6-311++G** level for different energy cutoffs (in cm^{-1}).

Cutoff	Gas	Solution
600	761	
800	774	
1000	784	1828
1200	793	1832
1400	801	1843
1600		1844
1800		1914

5. Conclusion

The vibrational spectra for $[(Py_2H)^+]$ were calculated at the B3LYP/6-311++G** level and the results were compared with the existing experimental data. According to our calculations, the bands at 1655 and 1255 cm^{-1} were assigned to the in-plane and out-of-planed N–H bending modes, respectively, which are quite different with those reported by Clements and Wood [7]. Furthermore, one-dimensional proton potential calculations indicate a barrier to proton movement of about 770 and 1400 cm^{-1} in the gas phase and solution, respectively.

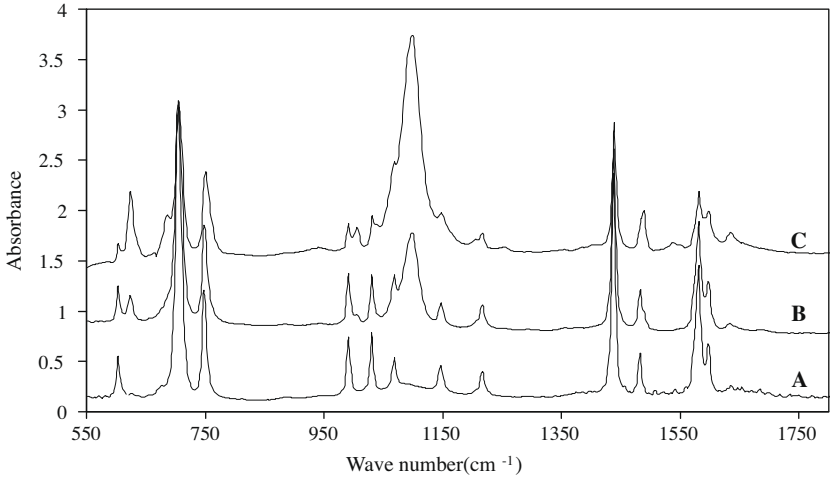

Fig. 6. Mid-range infrared spectra of pure pyridine (A), $(Py_2D)^+ClO_4^-$ (B), and $(Py_2H)^+ClO_4^-$ (C) in pyridine.

Acknowledgement

Y.A.W. gratefully acknowledges the financial support from the Natural Sciences and Engineering Research Council (NSERC) of Canada.

References

[1] L.C. Remer, J.H. Jensen, J. Phys. Chem. A 104 (2000) 9266.
[2] A. Novak, Struct. Bond. 18 (1974) 177.
[3] S.F. Tayyari, M. Zahedi-Tabrizi, F. Tayyari, F. Milani-Nejad, J. Mol. Struct. (THEOCHEM) 637 (2003) 171.
[4] S.F. Tayyari, M. Zahedi-Tabrizi, H. Rahemi, H.A. Mirshahi, J.S. Emampour, M. Rajabi, F. Milani-Nejad, J. Mol. Struct. (THEOCHEM) 730 (2005) 17.
[5] Th. Zeegers-Huyskens, P. Huyskens, in: H. Ratajczak, W.J. Orville-Thomas (Eds.), Molecular Interactions, vol. 2, Wiley, Chichester, UK, 1981, p. 1.
[6] E.N. Gur'yanova, I.P. Gol'dshtein, T.I. Perepelkova, Russ. Chem. Rev. 45 (1976) 792.
[7] R. Clements, J.L. Wood, J. Mol. Struct. 17 (1973) 283.
[8] J. Fritsch, G. Zundel, J. Chem. Soc., Faraday Trans. I 77 (1981) 2193.
[9] M.J. Frisch, G.W. Trucks, H.B. Schegel, G.E. Scuseria, M.A. Robb, J.R. Cheeseman, J.A. Montgomery Jr., T. Vreven, K.N. Kudin, J.C. Burant, J.M. Millam, S.S. Iyengar, J. Tomasi, V. Barone, B. Mennucci, M. Cossi, G. Scalmani, N. Rega, G.A. Petersson, H. Nakatsuji, M. Hada, M. Ehara, K. Toyota, R. Fukuda, J. Hasegawa, M. Ishida, T. Nakajima, Y. Honda, O. Kitao, H. Nakai, M. Klene, X. Li, J.E. Knox, H.P. Hratchian, J.B. Cross, V. Bakken, C. Adamo, J. Jaramillo, R. Gomperts, R.E. Stratmann, O. Yazyev, A.J. Austin, R. Cammi, C. Pomelli, J.W. Ochterski, P.Y. Ayala, K. Morokuma, G.A. Voth, P. Salvador, J.J. Dannenberg, V.G. Zakrzewski, S. Dapprich, A.D. Daniels, M.C. Strain, O. Farkas, D.K. Malick, A.D. Rabuck, K. Raghavachari, J.B. Foresman, J.V. Ortiz, Q. Cui, A.G. Baboul, S. Clifford, J. Cioslowski, B.B. Stefanov, G. Liu, A. Liashenko, P. Piskorz, I. Komaromi, R.L. Martin, D.J. Fox, T. Keith, M.A. Al-Laham, C.Y. Peng, A. Nanayakkara, M. Challacombe, P.M.W. Gill, B. Johnson, W. Chen, M.W. Wong, C. Gonzalez, J.A. Pople, Gaussian 03, Revision D01, Gaussian, Inc., Wallingford, CT, 2004.
[10] A.D. Becke, J. Chem. Phys. 97 (1992) 9173.
[11] A.D. Becke, J. Chem. Phys. 98 (1993) 5648.
[12] C. Lee, W. Yang, R.G. Parr, Phys. Rev. B. 37 (1988) 785.
[13] L. Onsager, J. Am. Chem. Soc. 58 (1936) 1486.
[14] M.W. Wong, K.B. Wiberg, M.J. Frisch, J. Am. Chem. Soc. 114 (1992) 1645.
[15] B.S. Furniss, A.J. Hanaford, P.W.G. Smith, A.F. Tatahall, Text Book of Practical Organic Chemistry, fifth ed., Addition Wiley Longmann Limited, 1989.
[16] GaussView 3.0, Gaussian Inc., Garnegie Office, Park, Pittsburgh, PA 15106.
[17] Genplot Package Computer Graphic Service, Cornel University, Utica, New York, 1990.
[18] J.A. Ibers, J. Chem. Phys. 41 (1964) 25.
[19] T.R. Singh, J.L. Wood, J. Chem. Phys. 48 (1968) 4567.
[20] E.B. Wilson, J.C. Decieus, P.C. Cross, Molecular Vibrations, McGraw-Hill, New York, 1955 (Appendix III).
[21] D. Cook, Can. J. Chem. 39 (1961) 2009.
[22] K.B. Wiberg, V.A. Walters, K.N. Wong, St.D. Colson, J. Phys. Chem. 88 (1984) 6067.
[23] F.P. Urena, M.F. Gomez, J.J.L. Gonzalez, E.M. Torres, Spectrochim. Acta A 59 (2003) 2815.
[24] I.G. Shenderovich, Russ. J. Gen. Chem. 77 (2007) 620.
[25] Ilia A. Guzei, John Roberts, Dovas A. Saulys, Acta Crystallog. Section C58 (2002) 141.
[26] Mariusz Makowski, Rafał Sadowski, Danuta Augustin-Nowacka, Lech Chmurzynski, J. Phys. Chem. A 105 (2001) 6743.